Random Flow Generation Technique for Large Eddy Simulations and Particle-Dynamics Modeling

A. Smirnov, S.Shi, I. Celik

Abstract

A random flow generation (RFG) technique is presented, which can serve as a subgrid-scale model in LES (Large-Eddy-Simulations) or RANS (Reynolds-Averaged Navier-Stokes) computations of turbulent flows. The technique allows to generate inhomogeneous anisotropic divergence free vector field representing turbulent velocity fluctuations. It was validated on the case of inhomogeneous anisotropic boundary layer flows. The applications of the technique in LES and in particle tracking applications are demonstrated.

Nomenclature

LES	Large Eddy Simulation
NS	Navier Stokes
RANS	Reynolds Averaged Navier Stokes equation
RFG	Random Flow Generation
PD	Particle Dynamics
l	Length scale of turbulence
τ	Time scale of turbulence

1 Introduction

In a Reynolds Averaged Navier-Stokes (RANS) turbulence modeling approach information about turbulent fluctuations is contained in the time averaged Reynolds stresses of the form $\overline{u_i u_j}$. These are obtained as an outcome of a turbulence model that links Reynolds Stresses to mean flow quantities (e.g. k-ϵ model), or solves modeled transport equations for each Reynolds stress component (e.g. Reynolds Stress models). However, this is not the case when the large eddy simulation (LES) methodology is employed since the goal here is to explicitly resolve the turbulent fluctuations. In LES the inlet conditions can not be derived directly from experimental results, because of the unsteady and pseudo-random nature of the flow being resolved, unless, off course, the turbulent intensity is zero at the inlet, which is rarely the case. This problem becomes more important for spatially developing turbulent flows where for example the boundary or shear layer thickness changes rapidly. In such cases periodic boundary conditions can not be specified unlike the fully developed channel flow (?; Akselvoll and Moin, 1995). A similar situation exists for prescribing the initial conditions over the whole calculation domain, if the turbulent flow is not steady in the mean (i.e. non-stationary turbulence) and the transients f the flow is to be resolved. Even for stationary turbulent flows, if realistic initial conditions are not prescribed, the establishment of the fully developed turbulence takes unreasonably long execution times. For these reasons is necessary to initialize the flow with some form of perturbation to provide an initial turbulent condition. It is important that the perturbation be spatially correlated, as is the case with the real flow. For external flow problems the turbulent flow field can be initiated simply by appropriately perturbing the inflow boundary conditions. In this case representing temporal correlations of the flow-field can be important. The inlet perturbation propagates throughout the flow field, which helps trigger the turbulence that is to be captured. Many applications of LES begin with initializing the flow field to that of a previously obtained RANS solution. A higher resolution grid is then used with an appropriate sub-grid-scale model. The Reynolds stress terms provided by the RANS solution can be used to provide spatially and temporally correlated perturbed inlet and initial conditions. It is possible to predict turbulence via LES technique, starting from a quiescent flow or with the mean flow obtained from RANS but it takes a very long time for a turbulent flow to develop spatially and temporally. This is especially true in the case of decaying turbulence in the absence of strong turbulence generating factors like walls. To remedy this problem the inlet and initial condition should consist of a mean component and a randomly fluctuating component with the appropriate statistics.

A work in this direction has been performed in the area of particle dispersion modeling with the RANS approach (Zhou and Leschziner, 1991; Zhou and Leschziner, 1996; Li et al., 1994). RANS modeling produces smooth flow fields, which do not accurately disperse particles that are embedded in the flow. The Reynolds stress terms are used to generate temporally and spatially correlated fluctuations such that instantaneous velocity fluctuations can be superimposed on the particles to induce realistic dispersion. Another approach found in the literature (Li et al., 1994) is based on generating an isotropic continuous flow-field proposed earlier by Kraichnan (1970). However, this flow-field does not satisfy the requirement of spatial inhomogeneity and anisotropy of turbulent shear stresses, which may be important in realistic flows. The method of Zhou and Leschziner (1991) complies with the latter requirement, but the resultant flow field does not satisfy the continuity condition and is spatially uncorrelated. For homogeneous isotropic turbulence, the initial conditions can be constructed as described by Ferziger (1983), The approach is based on vector curl operation and forward/backward Fourier transforms, which require a considerable computational effort. The extension of this method to anisotropic, inhomogeneous flows is not trivial.

It is the objective of this study to formulate a relatively simple random flow generation (RFG) algorithm which can be used to prescribe inlet conditions as well as initial conditions for spatially developing inhomogeneous, anisotropic turbulent flows. In principle the same procedure can also be used for initializing direct numerical simulations, but the focus of our study is on LES, and particle tracking. This method takes advantage of the previous work in the area of particle dispersion (Li et al., 1994). The RFG procedure is developed on the basis of the work of Kraichnan (1970) that can be used as an efficient random flow-field generator in LES and in particle tracking. The technique is illustrated on the example of bubbly ship-wake flow as one of the most challenging cases for LES and particle dynamics applications. Performing LES of ship wakes is particularly difficult given the fact that the whole ship must be modeled to capture the relatively thin 3D-boundary layer, preferably including the viscous sublayer. The boundary layer is the source of the flow dynamics that sets the initial conditions for the wake. A simulation that includes the whole ship and the wake would require prohibitively large computational resources. It is proposed here that the needed computational resources could be drastically reduced if an appropriate time-dependent inlet condition could be constructed at the beginning of the wake, thus avoiding the need to model the entire ship.

2 Methodology

To generate a realistic flow field we propose a modified version of Kraichnan's technique (Kraichnan, 1970). The procedure we call RFG (Random Flow Generation) combines the advantages of the approaches mentioned above and is also computationally efficient. It involves scaling and orthogonal transformations applied to a continuous flow-field generated as a superposition of harmonic functions. The procedure consists of the following steps.

1. Given an anisotropic velocity correlation tensor

$$r_{ij} \equiv \overline{\tilde{u}_i \tilde{u}_j} \tag{1}$$

of a turbulent flow field $\{\tilde{u}_i(x_j,t)\}_{i,j=1..3}$, find an orthogonal transformation tensor a_{ij} that would diagonalize r_{ij} [1]

$$a_{mi}a_{nj}r_{ij} = \delta_{mn}v'^2_{(n)} \tag{2}$$

$$a_{ik}a_{kj} = \delta_{ij} \tag{3}$$

As a result of this step both a_{ij} and v'_n become known functions of space.

2. Generate a transient flow-field in a three-dimensional domain $\{v_i(x_j,t)\}_{i,j=1..3}$ using the modified method of Kraichnan (Kraichnan, 1970)

$$v_i(\vec{x},t) = \sqrt{\frac{2}{N}}\sum_{n=1}^{N}[p_i^n \cos(\tilde{k}_j^n\,\tilde{x}_j + \omega_n\tilde{t}) + q_i^n \sin(\tilde{k}_j^n\,\tilde{x}_j + \omega_n\tilde{t})] \tag{4}$$

$$\tilde{x}_j = \frac{x_j}{l},\ \tilde{t} = \frac{t}{\tau},\ v' = \frac{l}{\tau},\ \tilde{k}_j^n = k_j^n\frac{v'}{v'_{(j)}} \tag{5}$$

$$p_i^n = \varepsilon_{ijm}\zeta_j^{(n)}k_m^{(n)},\ q_i^n = \varepsilon_{ijm}\xi_j^{(n)}k_m^{(n)} \tag{6}$$

$$\zeta_i^n,\ \xi_i^n,\ \omega_n \in N(0,1),\ k_i^n \in N(0,1/2),$$

where l, τ are the length and time-scales of turbulence, ε_{ijk} is the permutation tensor used in vector product operation (Spain, 1965), and $N(M,\sigma)$ is a normal distribution with mean M and standard deviation σ. Numbers k_j^n, ω_n represent a sample of n wavenumber vectors and frequencies of the modeled turbulence spectrum

$$E(k) = 16(\frac{2}{\pi})^{1/2}k^4\,\exp(-2k^2) \tag{7}$$

[1] $f_{,i} \equiv \frac{\partial f}{\partial x_i}$. Repeated indexes imply summation, parentheses around indexes preclude summation.

3. Apply a scaling and orthogonal transformations to the flow-field v_i generated in the previous step to obtain a new flow-field u_i

$$w_i = v'_{(i)} v_{(i)} \tag{8}$$
$$u_i = a_{ik} w_k \tag{9}$$

The procedure above takes as an input the correlation tensor of the original flow-filed r_{ij} and information on length- and time-scales of turbulence (l, τ). As will be shown below, the time dependent flow-field $u_i(x_j, t)$ generated by the procedure is nearly divergence-free, with the correlation functions equal to r_{ij}. By virtue of Eq.(4), spatial and temporal variations of u_i follow Gaussian distribution with characteristic length and time-scales of l, τ, however, other probability density functions (PDF) can be used to simulate different problems.

It should be noted that random spectrum sampling in Eq.(6) can be performed separately from the actual assembly of the vectors in Eq.(4). This leads to a higher computational efficiency, since the spectrum sampling can be done outside of the main time iteration loop of the flow solver with only the assembly of fluctuating velocity components left inside the time loop. This efficiency comes at a price of extra memory requirements for storing the random sample. The size of this sample is equal to $10 \cdot N$, where N is the number of harmonic functions representing the turbulent spectrum in (4), which is independent of the actual grid size. So, for $N = 1000$ and double precision arithmetics only $80\,KB$ of computer memory will be needed to store the spectrum for any grid size.

Equation (8), provides the scaling, and (9) - the orthogonal transformation. Scaling factors v'_i obtained in step 1 represent the scales of turbulent fluctuations along each axis. They do not depend on time, whereas vectors v_i and w_i represent time-dependent velocity fluctuations. By construction, the correlation tensor of the flow-field produced by Eq.(4) is diagonal

$$\overline{v_i v_j} = \delta_{ij} \tag{10}$$

The flow-field w_i produced after the scaling transformation (8) is nearly divergence free, as is given by the following estimate

$$\begin{aligned} w_{i,i} &\approx v'_i v_{i,i} = \\ = \frac{v'}{l}\sqrt{\frac{2}{N}} \sum_{n=1}^{N} [p_i^n\, k_i^n \cos(\frac{v'}{v'_j} k_j^n \frac{x_j}{l} &+ \omega_n \frac{t}{\tau}) \\ + q_i^n\, k_i^n \sin(\frac{v'}{v'_j} k_j^n \frac{x_j}{l} &+ \omega_n \frac{t}{\tau})] = 0 \qquad (11) \\ \Longrightarrow \quad w_{i,i} &\approx 0 \qquad (12) \end{aligned}$$

where we neglected all derivatives of v'_i, which are slowly varying functions of $\vec{x}$, and used the relation of orthogonality between k_i^n and p_i^n, q_i^n

$$k_i^{(n)}\, p_i^{(n)} = k_i^{(n)}\, q_i^{(n)} = 0$$

which follows from the way vectors p_i^n, q_i^n are constructed in (6). Since both a_{ij} and v'_i are determined by r_{ij} they will be functions of space[2] as long as flow is inhomogeneous. Because of the averaging

[2]Since r_{ij} is produced by averaging (Eq.1) it does not depend on time

operation involved in obtaining r_{ij} (Eq.1) the length-scale of change of $r_{ij}(\vec{x})$ is substantially greater than that of the instantaneous velocity $u_i(\vec{x},t)$. In particular, it means that $\|\nabla(u_i u_i)\| \gg \|\nabla r_{ij}\|$, where $\nabla f \equiv f_{,i}$ and $\|\cdot\|$ to denotes an appropriate function norm. Since a_{ij} are derived from r_{ij} the same estimate is valid for a_{ij}, namely

$$\|\nabla a_{ij}\| \ll \|\nabla(u_i u_i)^{1/2}\| \tag{13}$$

This in turn means that the divergence-free property of the original flow field a_{ij} Eq.(12) will be preserved by the orthogonal transformation (9)

$$u_{i,i} = a_{ij}a_{ki}w_{j,k} = \delta_{jk}w_{j,k} = w_{j,j} = 0 \tag{14}$$

where we used relation (12) and the rule of transformation of derivatives: $f'_{,i} = a_{ji}f_{,j}$. Thus, the generated flow-filed u_i is divergence-free within the accuracy determined by (13). At the same time the new flow field satisfies the anisotropy of the original flow-field $\vec{u}(\vec{x},t)$, i.e.

$$\begin{aligned} \overline{u_i u_j} \ &= \ \overline{a_{im}w_m\, a_{jn}w_n} \ = \\ a_{im}a_{jn}\overline{w_m\, w_n} \ &= \ a_{im}a_{jn}v'_m v'_n\overline{v_m\, v_n} \ = \\ a_{im}a_{jn}v'_m v'_n\delta_{mn} \ &= \ a_{im}a_{jn}\delta_{mn}(v'_n)^2 \ = \ r_{ij} \end{aligned} \tag{15}$$

Where we used relations (3), (8) and the last equality was obtained by solving (2) for r_{ij}. Thus, the obtained flow-field $u_i(\vec{x},t)$ is transient, divergence-free, inhomogeneous, and anisotropic with the pre-defined correlation coefficients.

The RFG procedure can be extended to include the anisotropy of turbulence length-scale. In this case instead of using a scalar value for l in (5) one can define a vector l_i^{turb}. In this case an appropriate rescaling is necessary to preserve the continuity of the flow-field. This is done by introducing another scaling transformation, similar to (8), which will guarantee that the resultant flow-field is divergence-free.

3 Validation of RFG procedure

The first test of the procedure was for a homogeneous isotropic flow field. The Fourier space was sampled with 1000 wave-numbers selected according to Eq. (4). Figure 1 shows the snapshot of a homogeneous isotropic velocity field. Fig.1(a) shows the vorticity field in a cross-section of the computational domain, and in Fig.1(b) the velocity distribution is presented. Statistical post-processing of velocity correlations was applied to the generated flow-field in order to verify that the velocity field was isotropic. For that purpose a turbulent flow-field with the characteristic time scale of $10^{-3}\,s$ was generated from the Fourier spectral sample of 1000 wave-vectors (Eq.4). The fluctuating velocities were sampled at the rate of $10^5\,Hz$. Correlations of the fluctuating velocity components were computed at one point in space by averaging over time. Fig.6 shows the behavior of the velocity correlations as a function of the averaging time-interval. The figure indicates convergence to the values corresponding to Eq.(10).

The procedure was next applied to a homogeneous anisotropic flow field with v'_i selected from typical boundary layer distributions. This type of anisotropy leads to higher amplitudes of the velocity vectors in one direction relative to the other (Fig.2(a)). The procedure was also used to generate the flow-field with anisotropic length-scales (see comments in Sec.2). In this case the length-scale of fluctuations was selected differently in different spatial directions. This produced a flow-field where the structure of the velocity fluctuations seemed stretched in one direction (Fig.2(b)).

The last test performed was for a non-homogeneous anisotropic boundary layer. Figure 3 shows a snapshot of the velocity magnitude in the three-dimensional boundary layer. An additional empirical factor related to the boundary-layer thickness was introduced in this case to better account for the intermittency effects. Figure 4 shows the random signal produced by the RFG procedure sampled at different locations above the boundary plane. As can be seen from that figure both anisotropy and inhomogeneity are evident in the fluctuating components. Experimental and direct numerical simulation (DNS) data do exist for this flow field, providing both mean and fluctuating velocity profiles, as well as turbulent correlations. The turbulent boundary layer is two-dimensional in the mean, though turbulent fluctuations exist in all three dimensions denoted in this report as u', v', and w' for the axial, vertical, and tangential directions, respectively. In addition, the correlation involving the axial and vertical velocity fluctuations is significant. The Reynolds stresses were obtained from (Hinze, 1975) where the classical experiments of Klebanoff (1954) are summarized.

A number of realizations N_T of the boundary layer was computed using the turbulence time scale of $t_{turb} = 10^{-3}\,s$, length-scale of $l_{trub} = 10^{-3}$, and a sample size of 1000 harmonic functions. The wave-vectors for these functions were taken from a normal distribution with the mean $\sim t_{turb}^{-1}$. The boundary layer thickness (δ) was allowed to grow according to the following empirical relation:

$$\delta = 0.16 \cdot x \cdot \left(\frac{U_0 x}{\nu}\right)^{-1/7} = 0.16 \cdot x \cdot Re_x^{-1/7} \tag{16}$$

where x is the axial distance and U_0 is the free-stream velocity, which was set equal to $1.0\,m/s$. The cross correlation ($\overline{uv}$) was normalized with the friction velocity U_τ, which is itself a function of U_0. The boundary layer thickness was randomly perturbed with a continuous function using the same spectral sampling technique as for the velocity fluctuations to emulate intermittency.

Fig.5 shows the vorticity field of the generated boundary layer flow-field compared with LES data (Speziale, 1998). As can be seen from the figure, by choosing the turbulence length-scale correctly, one can achieve a good resemblance in the flow structure simulated with this semi-analytic approach and a LES flow-field.

To compare the simulation results with the experimental data the velocity profile along a vertical line in the center of the axial plane was stored for each simulated realization of the flow-field. The profiles of the thousand time realizations were then used to calculate the average fluctuating components in each direction, as well as the corresponding cross correlations. These are compared to the original experimental data in the Figure 7. As can be seen, the experimental data is well reproduced.

The divergence-free property of the generated flow-filed was tested by computing the divergence as a function of turbulence length-scale for three cases: isotropic velocity field, generated according to the original Kraichnan method (Kraichnan, 1970; Li et al., 1994), anisotropic velocity field, generated according to the modified Kraichnan method, using Eqs.(4)-(5) with $\tilde{k}_j^n \equiv k_j^n$, and anisotropic velocity field generated according to the RFG algorithm based on Eqs.(2)-(9). For this test case the anisotropy of different fluctuating velocity components was selected to be given by a ratio: $0.1 : 1.4 : 1$ for v_1', v_2', and v_3' respectively.

The divergence test was done on a cubic grid. For each grid-cell the divergence was computed as the sum of fluxes through cell faces. The Fourier space was sampled with 1000 wave-numbers selected according to Eq. (4). Fig.8 depicts the computed divergence as a function of the ratio of turbulence length-scale l to grid cell size. The result represents an average over 10,000 realizations of the flow-field. As can be seen from the figure in all three cases the continuity error decreases with the increase of the turbulence length-scale. This decrease is considerably slower for the anisotropic flow-field generated according to the original Kraichnan method compared with the the cases of isotropic flow field and anisotropic flow generated with RFG procedure. It should be noted that the theoretical continuity error in the isotropic case is zero. The discrepancy between this case and the anisotropic case computed with the Kraichnan method is due to the violation of continuity of that method in the presence of anisotropy. In contrast, the flow-field produced with the new RFG procedure has practically the same as for the isotropic case. This means that the anisotropic flow-field generated by the RFG procedure is essentially divergence free. At the same time is shows the importance of scaling transformation for k_j^n in (5) for the fulfillment of continuity. The upper divergence limit in the figure occurs when the grid cell-size is comparable or greater than turbulence length-scale l. It is due to the integration errors, which in this limit case can be estimated from the relation $\|\overline{u_i u_j}\| \approx 1$.

4 Applications

The RFG procedure offers a relatively inexpensive way to generate random velocity fluctuations, representing a turbulent flow-field. Since the generated velocity field satisfies the relations of continuity and anisotropy it is a far more realistic representation of turbulence than can be obtained with a simple Gaussian velocity distribution using a random-number generator. Because the flow-field produced by RFG may not satisfy the momentum equations it is still an approximation. However, in some applications this approach may offer a simple and reasonably accurate way to model turbulence without solving the complete Navier-Stokes (NS) equation, which would require much more memory and execution time. The RFG procedure also provides a flexibility of a trade-off between the accuracy of representing a turbulent spectrum and memroy/time requirement. By increasing the spectral sample size N in (4) one can increase the accuracy of reproducing the turbulent spectrum at the cost of longer execution time and higher memory utilization. In addition to that, since the velocity field is calculated by analytical functions (Eq.4), it is given at any point in space and time, and not just at the grid nodes for some discrete time values. Because of this quality, the method can be used as a subgrid-scale model for LES or RANS simulations and in modeling turbulent particle-laden flows.

As an illustration of the technique we applied it together with the RANS method to simulate turbulent fluctuations in a ship wake. The high-Reynolds number character of ship wakes ($R_e \sim 10^7 - 10^8$) makes it rather time-consuming to perform full-scale LES of these flows. In this situation a combination of a RANS method and RFG technique can offer an efficient way to produce a time-dependent turbulent flow-field. Figure. 9 shows a snapshot of an unsteady turbulent flow-field around a ship-hull produced as a superposition of the mean flow velocity, computed with a RANS method ($k - \epsilon$) (Larreteguy, 1999) and the fluctuating velocity obtained with the RFG procedure. This unsteady flow-field can be used for the analysis of flow-structure ineractions and/or particle tracking (see Sec. 4.1).

4.1 Particle dynamics modeling

Particle tracking in transient flows is usually a time-expensive computational procedure. In the situations when the turbulent flow is computed using RANS models it is possible to compute particle dynamics in a steady-state mean flow field and add a fluctuating component to the particle velocities. When LES technique is used the particles should follow a time-dependent flow-field and the fluctuating component should still be added to it at smaller turbulence scales. In both cases the fluctuating component is derived from the turbulence intensity and length-scales, provided by the turbulence model.

4.1.1 Particle-dynamics in a turbulent flow

We shall continue with a ship-wake flow as an illustrative example of particle-tracking application in turbulent high-Reynolds-number flows. Simulations of bubbles in ship wakes requires account of several processes, like drag, lift and buoyancy forces, bubble dissolution in water, bubble interaction with the free-surface (including bubble disappearance at the surface and bubble generation due to air entrainment). In some cases, because of uneven bubble distribution (e.g. local clustering), the coalescence and/or breakup of bubbles may be important. Because of this non-uniformity, sharp gradients in bubble concentration, and low volume fraction of the bubbles Lagrangian approach to model bubble dynamics is often preffered. Compared to the two-fluids method (Elghobashi, 1994; Crowe, 1998) the Lagrangian approach requires less empiricism and is more suitable for parallel implementation. We use a particle dynamics (PD) algorithm based on efficient particle tracking, population dynamics and a novel particle interaction techniques (Smirnov et al., 2000).

To simulate bubbles in a ship-wake we use the combination of RFG and PD algorithms. Fluid velocity at the location of every bubble was approximated as a sum of the mean fluid velocity obtained from the RANS calculations and the fluctuating part computed with the RFG procedure. Since RANS solution is given only at the Eulerian grid-node locations and bubbles follow Lagrangian trajectories, an interpolation is required to approximate the mean velocity at bubble's current location. No such approximation is necessary for the fluctuating part, since the RFG procedure defines a flow-field at every point in space and time. In the simulation the bubbles were injected at a single point close to the ship hull where the turbulent kinetic energy was near its maximum (Fig. 10). Only drag and buoyancy were included at this point. Considering the importance of some of other forces for a realistic bubble dynamics, specifically virtual-mass terms (Crowe et al., 1998), we will not use the term "bubbles" in what follows but rather refer to them as "particles". This simplification is justified for the present purpose of testing the performance of RFG algorithm. A total of $10\ 000$ particles of 100 microns in diameter were continuously injected into the domain. Two seconds of real-time were simulated for the ship-length of $6m$ traveling with the speed of $3m/s$. The figure shows the tendency of particles to agglomerate in dense groups. The characteristic sizes of these groups are in many instances smaller than the grid-cell size. This reflects the very sub-grid nature of the RFG method, which enables to capture finer details of particle dynamics than can be resolved on an Eulerian grid.

4.2 Large-Eddy Simulations (LES)

In Large Eddy Simulations the RFG procedure can be used to generate random inflow-conditions or serve as a subgrid-scale model. There is an extensive literature regarding LES techniques (Piomelli, 1999). To reach a state of developed turbulence in LES simulations require a substantial computational time. Regarding this there are two important problems in LES of a high-Reynolds number turbulence that can be solved with the RFG procedure: (1) assigning initial flow-field distribution and (2) assigning turbulent inflow conditions. Conventionally, the first problem is dealt with by increasing the transition phase of the simulation and the second - by extending the size of the computational domain. Consequently, the remedy comes at a price of a longer execution time and higher memory requirements. By using a RFG procedure to generate the initial conditions one can cut down on the execution time considerably. For stationary turbulence the approximate nature of the initial velocity distribution with respect to the solution of the NS-equation is of little significance, since these discrepancies are corrected in the first few iterations of the NS-solver.

The problem of inlet conditions could be even more important, since extending the computational domain will increase both execution time and memory requirements of the simulation. In this case RFG can provide reasonable inflow conditions with the pre-determined anisotropy properties. Here again we illustrate these advantages on the example of a ship wake. A complete LES simulation of the wake would normally require simulating the unsteady flow around the ship hull and in the wake region. Enploying the RFG procedure for the inlet conditions, we can restrict LES run to the near wake region only. In this case the information on turbulence levels and anisotropy at the inlet plane, required by RFG, can be obtained from relatively inexpensive RANS calculations.

This approach was applied to the wake of a model ship (Navy 5415 model (Carrica et al., 1998)). The inflow boundary is constructed by using the data from RANS calculations (Larreteguy, 1999). The turbulent normal stresses are based on the kinetic energy. The time scale and length scale which are used in generation of the perturbation at the inlet plane are selected from the corresponding relation between the turbueInt kinetic energy and its dissipation rate provided by the RANS calculations.

Figure 11 shows the instantaneous streamwise velocity contours and vertical vorticity contours, respectively, in a plane parallel to the free surface, where some of the the turbulence structures in the wake can be observed. Small-scale turbulent structures can be seen in both figures in the near wake region. These structures tend to increase in the far wake. This can be due to the following two factors: (1) In the very near wake, fine grids are applied so that smaller turbulence structures are captured. (2) Physically, larger tubulence structures include more energy so that they can last longer, while smaller turbulence structures have less energy and die quickly thus dissipating turbulent kinetic energy. Another phenomenon is the increase of the width of the wake in the downstream direction. The mean velocity profile (not shown here) also supports this result. Capturing of these phenomena supports the validity of our approach of computing the inflow boundary.

5 Conclusions and future work

The analytical method of Kraichnan (1970) was modified to account for the effects of inhomogeneity and anisotropy of turbulent shear stresses. The technique was realized in an efficient random field generation algorithm which was tested on the cases of isotropic turbulence, channel flow anisotropic flows, and boundary layer inhomogeneous anisotropic turbulence (Celik et al., 1999). The simulated flow fields are transient in nature and to a good approximation satisfy the conditions of continuity, anisotropy and inhomogeneity.

Advancing the realistic LES run to the stage of developed turbulence may require days of computation time[3]. Similarly, to obtain realistic turbulent inflow conditions may require the extention of the computational domain with the corresponding increase in computer time and memory requirements. The technique above can be used to generate the initial conditions in the matter of hours and continuously supply the turbulent inlet conditions close to the domain of interest, thereby reducing time and memory requirements of the LES simulations.

This study showed the feasibility of applying a hybrid LES technique in combination with RFG algorithm to high-Reynodls number flows, like those of ship wakes. It is also shown that the new

[3] Our benchmarking was performed on the 533 MHz DEC-Alpha processor

technique can be used effectively in conjunction with a Lagrangian particle dynamics approach is appropriate for bubble tracking in the wake and can be easily incorporated into LES codes.

In other applications sampling from a more realistic turbulence spectrum instead of the Gaussian (or *normal*) spectrum in step 2 of the procedure described above can be used.

Acknowledgements:

This work has been performed under a DOD EPSCoR project sponsored by the Office of Naval Research(ONR), Grant No.N00014-98-1-0611. The program officer is Dr. Edwin P. Rood. We thank professor Robert Street of Stanford University who kindly provided us with the basic code for LES. We also thank Dr.Calhoun and Mr.Li Ding in Stanford University for their suggestions about using the code.

References

Akselvoll, K. and Moin, P.: 1995, Technical Report TF-63, Stanford University

Carrica, P., Bonetto, D., Drew, D., and Lahey, R.: 1998, The interaction of background ocean air bubble with a surface ship, *Int.J.Numer.Meth.Fluids* **28**, 571

Celik, I., Smirnov, A., and Smith, J.: 1999, Appropriate initial and boundary conditions for LES of a ship wake, in *3rd ASME/JSME Joint Fluids Engineering Conference*, Vol. FEDSM99-7851, San Francisco, California

Crowe, C.: 1998, An assessment of multiphase flow models for industrial applications, in *Proceeding of FEDSM'98*, Vol. FEDSM-5093, Washingtow,DC,USA

Crowe, C., Sommerfeld, M., and Tsuji, Y.: 1998, *Multiphase Flows with Droplets and Particles*, CRC Press

Elghobashi, S.: 1994, On predicting particle-laden turbulent flow, *Applied Scientific Research* **52**, 309

et al., R.: 2000, *AIAA Paper* (2000-0542)

Ferziger, J.: 1983, Higher-level simulations of turbulent flows, in J. Essers (ed.), *Computational Methods for Turbulent Transsonic and Viscous Flows*, pp 93–183, Hemisphere Publishing Co., Springer Verlag

Hinze, J.: 1975, *Turbulence, 2nd edition*, McGraw-Hill, New York

Klebanoff, P.: 1954, *NACA Tech. Notes* 3133

Kraichnan, R.: 1970, Diffusion by random velocity field, *Phys. Fluid* **11**, 43

Larreteguy, A.: 1999, *Ship-Wake simulations*, Private communication

Li, A., Ahmadi, G., Bayer, R., and Gaynes, M.: 1994, Aerosol particle deposition in an obstructed turbulent duct flow, *J. Aerosol Sci.* **25(1)**, 91

Piomelli, U.: 1999, Large-eddy simulation: achievements and challenges, *Progress in Aerospace Sciences* **35**, 335

Smirnov, A., Shi, S., and Celik, I.: 2000, Random flow simulations with a bubble dynamics model, in *ASME Fluids Engineering Division Summer Meeting*, No. 11215 in FEDSM2000

Spain, B.: 1965, *Tensor Calculus*, Oliver and Boyd

Speziale, C.: 1998, Turbulence modeling for time-dependent RANS and VLES: a review, *AIAA Journal* **36(2)**, 173

Zhou, O. and Leschziner, M.: Sept. 1991, A time-correlated stochastic model for particle dispersion in anisotropic turbulence, in *8-th Turbulent Shear Flows Symp.*, Munich

Zhou, Q. and Leschziner, M.: 1996, *Modelling particle Dispersion in Turbulent Recirculating Flow with an Anisotropy- Resolving Scheme*, Technical Report TFD/96/07, UMIST

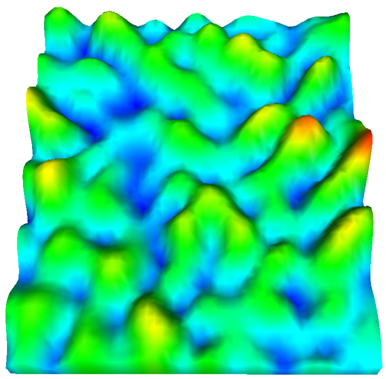

(a) Vorticity

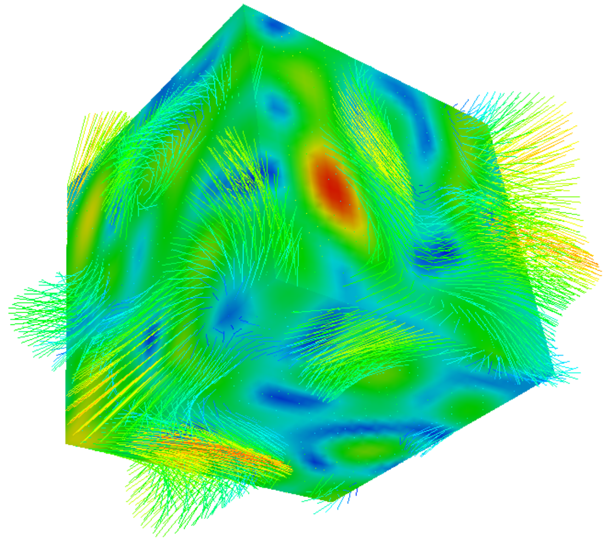

(b) Velocity

Figure 1: Isotropic homogeneous flow-field

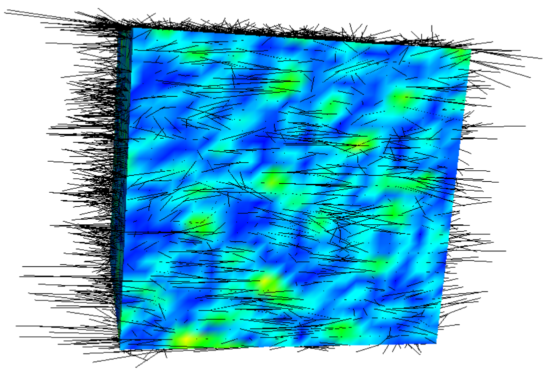

(a) Anisotropic velocity

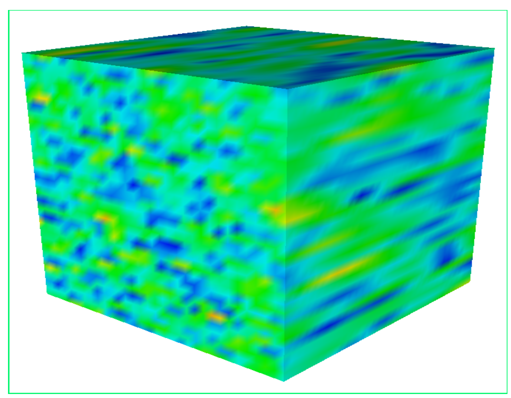

(b) Anisotropic length-scale

Figure 2: Anisotropic homogeneous flow-field

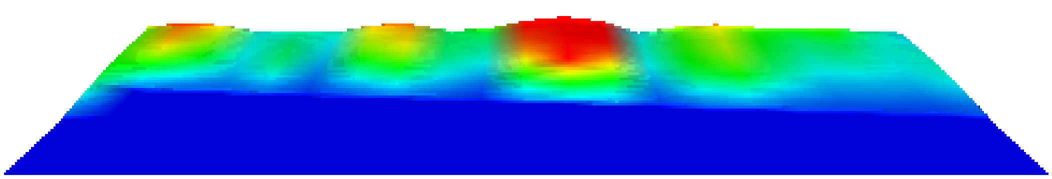

Figure 3: Fluctuating velocity in the boundary layer (RFG)

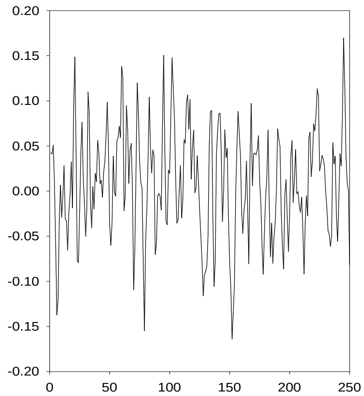

(a) Axial, $y/\delta = 0.13$

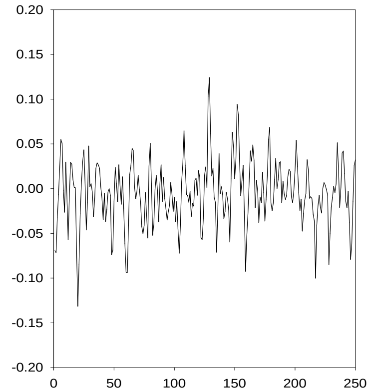

(b) Vertical, $y/\delta = 0.13$

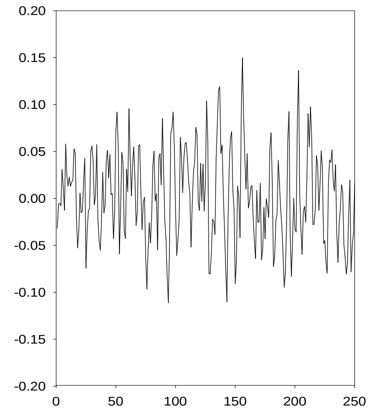

(c) Tangential, $y/\delta = 0.13$

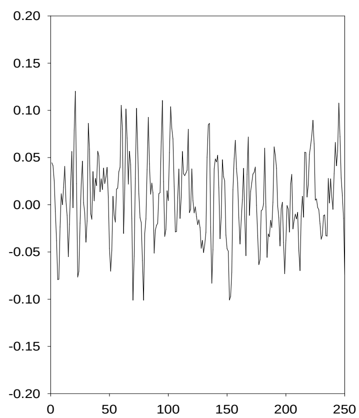

(d) Axial, $y/\delta = 0.46$

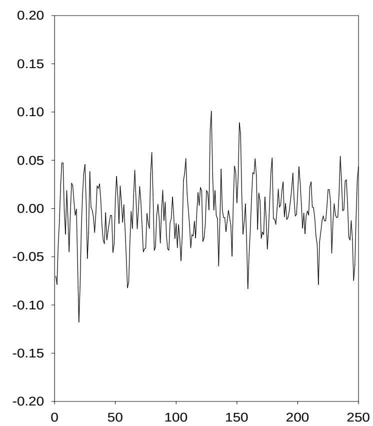

(e) Vertical, $y/\delta = 0.46$

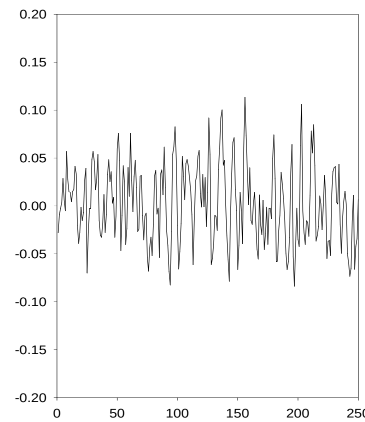

(f) Tangential, $y/\delta = 0.46$

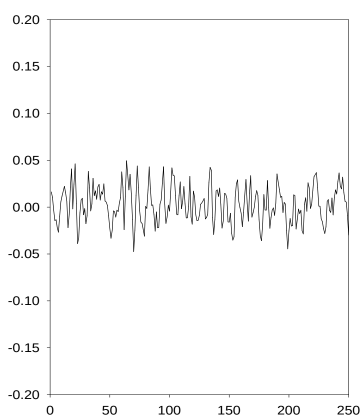

(g) Axial, $y/\delta = 0.76$

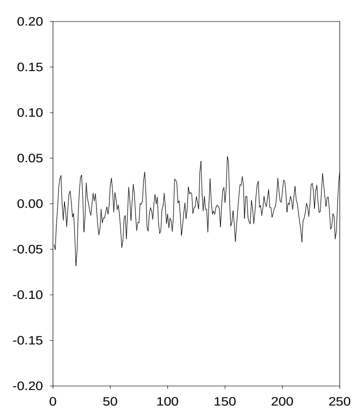

(h) Vertical, $y/\delta = 0.76$

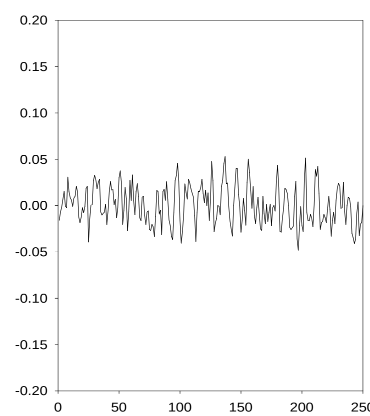

(i) Tangential, $y/\delta = 0.76$

Figure 4: Instantaneous velocity vs time step at different locations y/δ

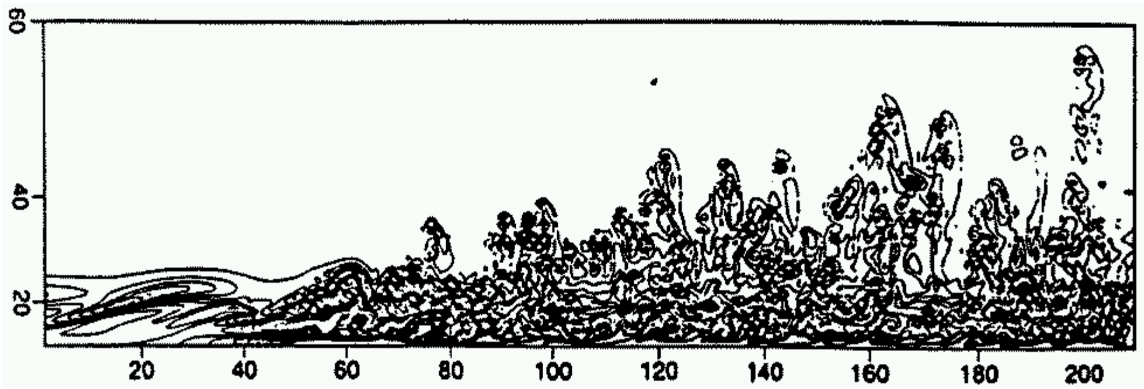

(a) LES (Speziale, 1998)

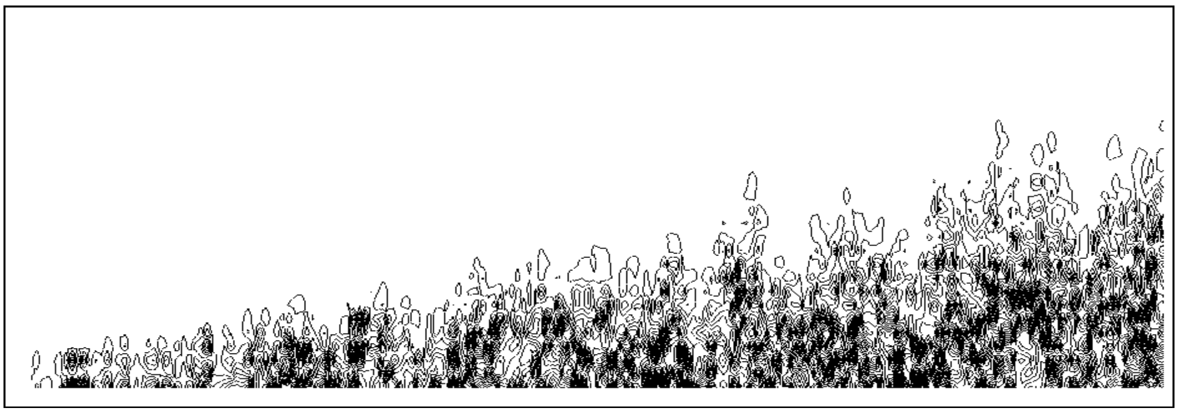

(b) RFG (large length-scale)

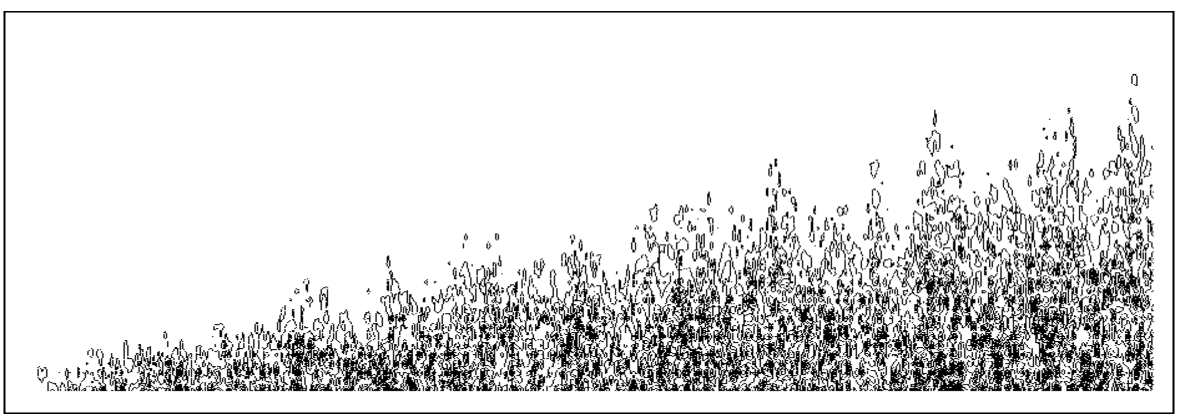

(c) RFG (small length-scale)

Figure 5: Vorticity contours in the boundary layer

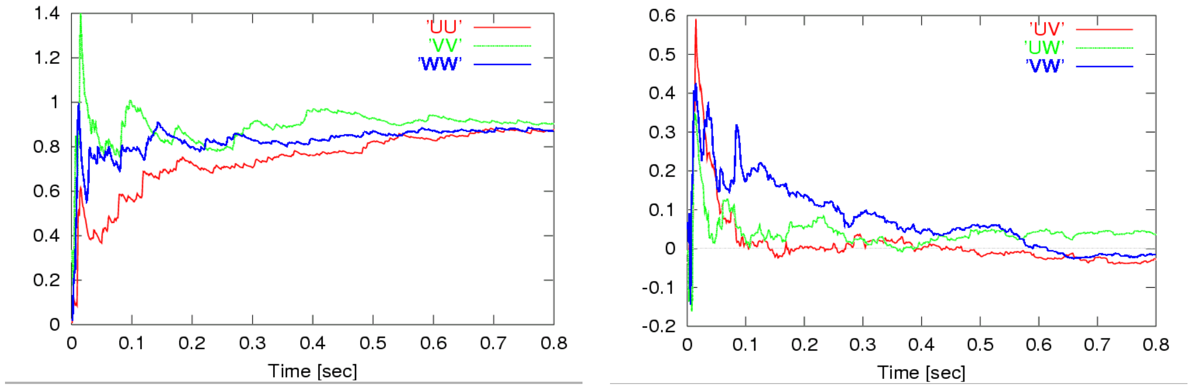

(a) Diagonal correlations

(b) Cross correlations

Figure 6: Convergence of velocity correlations

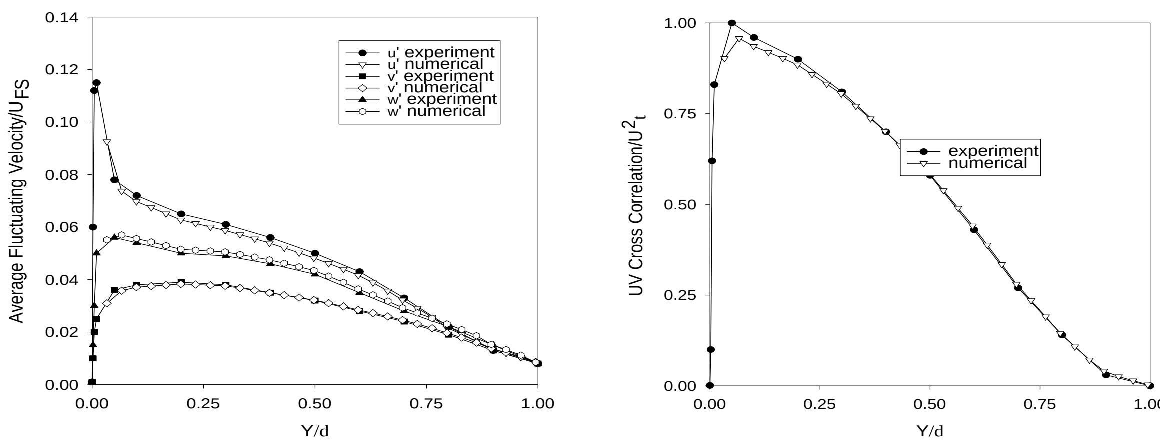

(a) Fluctuating velocities

(b) Axial/vertical cross correlations

Figure 7: Comparison with experimental data

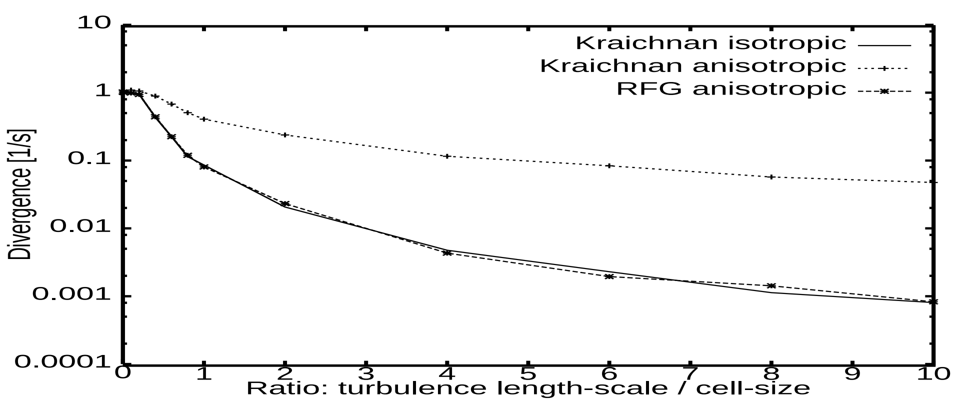

Figure 8: Normalized divergence of an anisotropic velocity field

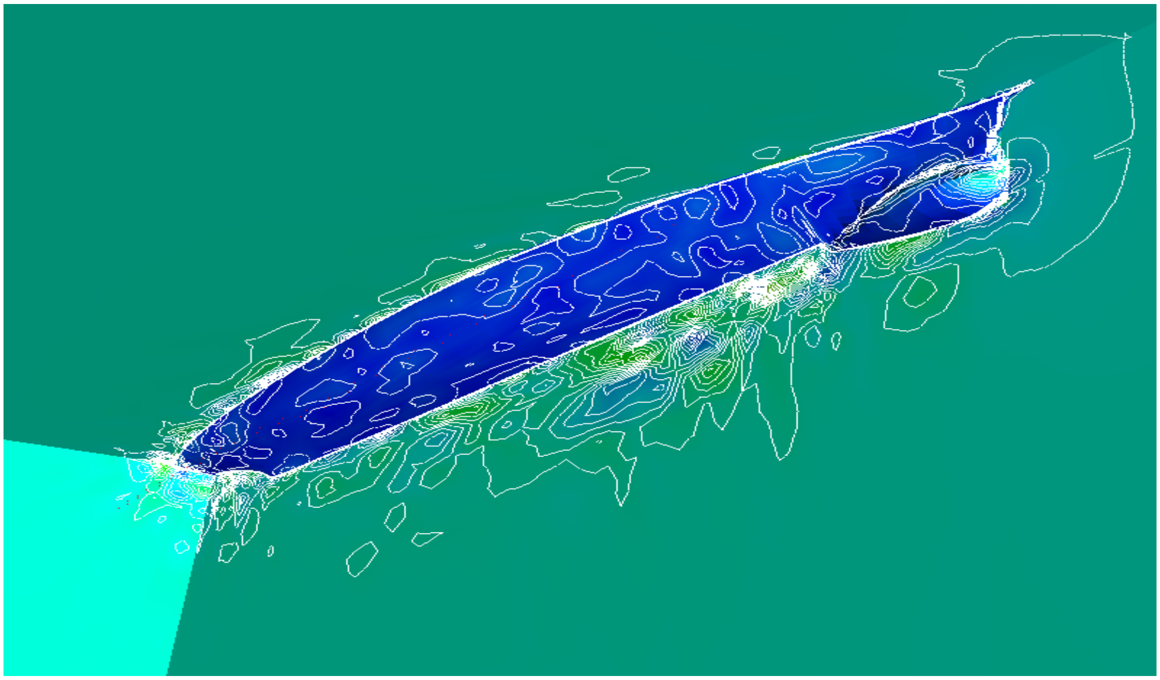

Figure 9: Turbulent velocity around a ship hull computed with the RFG algorithm.
View from below.

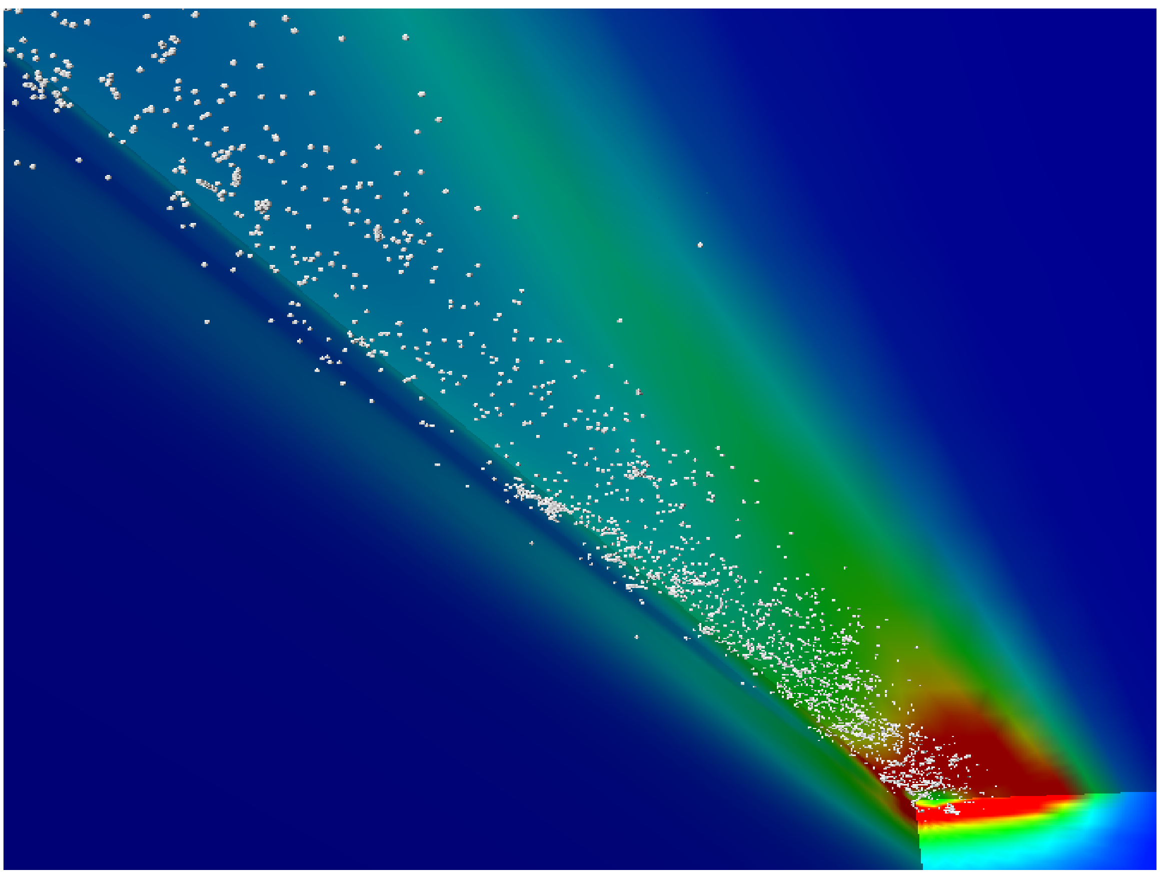

Figure 10: Bubbles in a ship-wake.
Background shading is according to the turbulent kinetic energy.

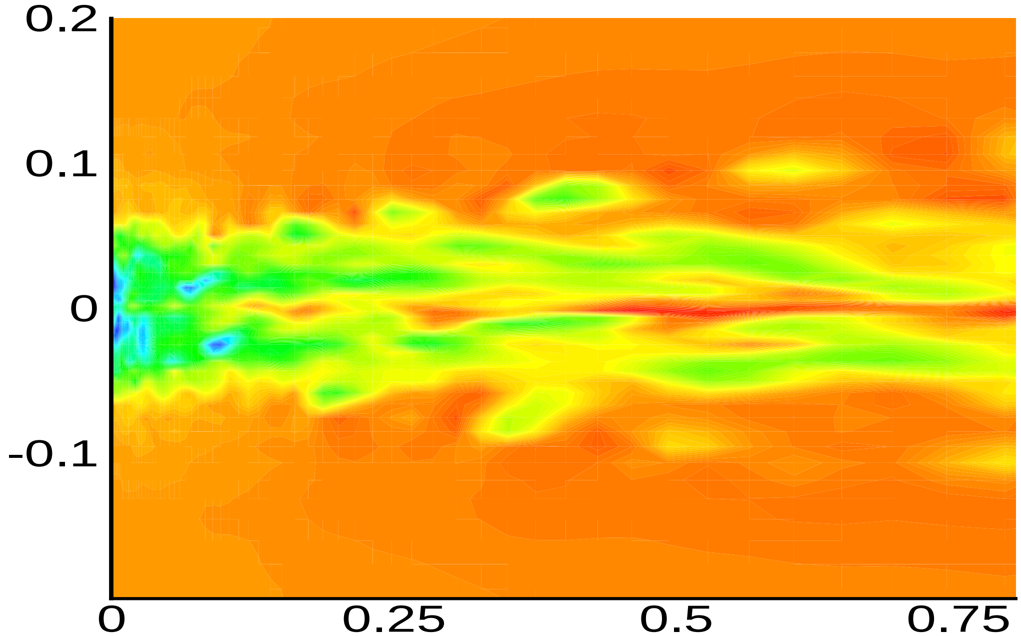

(a) Streamwise velocity countours of the simulated wake flow

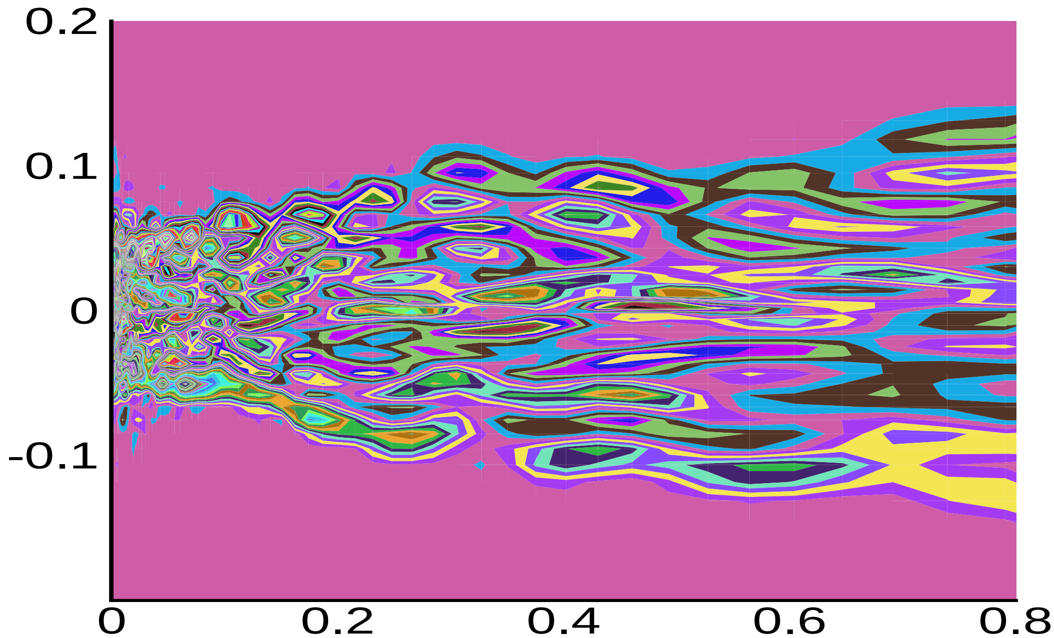

(b) Instantaneous vertical vorticity contours

Figure 11: LES of a ship-wake flow